whole medium (Fig. 1, G and H); thus, from two spirals only one is left. (iv) The spirals drift toward higher light intensity, as predicted in (*13*), which can be seen from a comparison of the tip position at different times; the drift is screw-like, as it is accompanied by the rotating motion of the spiral tip. The mean velocity of the drift has one component in the direction of the light gradient and another one perpendicular to it. The mean drift velocity, which can be estimated by comparing Fig. 1G with Fig. 1H, is 1.7×10^{-2} cm/min. (v) Strong deviations from the Archimedean spiral occur, the wavelength becoming larger in the regions with lower light intensity.

Figure 2 shows the automaton simulations corresponding to the experiments of Fig. 1. In agreement with these experimental results, the simulations yield instability in which the symmetry of the spiral pair is lost; the wavelength is enhanced; a spiral pair is transformed into a single spiral; there is spiral drift; and the system deviates from the Archimedean shape.

In order to quantify the automaton results, it is necessary that the iteration step and the length of a cell be expressed in physical time and space units. This can be done by comparing the period T and the wavelength λ of a spiral in homogeneous light (Figs. 1A and 2A). Experiments yield $T = 1.5$ min and $\lambda = 0.23$ cm. Simulations render $T = 7$ steps and $\lambda = 31$ cells. Thus, one iteration step corresponds to 0.21 min and one cell automaton is 7.4×10^{-3} cm long. The mean drift velocity, estimated by comparing Fig. 2G with Fig. 2H, is 0.53 cells per step, which in physical units is 1.9×10^{-2} cm/min, in good agreement with the experimental value of 1.7×10^{-2} cm/min obtained above.

An experiment with a radial gradient is shown in the upper pictures of Fig. 3; the corresponding automaton simulations are displayed below. Both in experiments and in simulations we observed that spirals straighten up, leading to uncurled wave ends. Also, we observed partial breaking of wave fronts into pieces. At the end of the experiment the mean drift velocity of the spiral tip is 5.9×10^{-2} cm/min, 3.5 times the velocity for the axial light gradient (Fig. 1). This is in good agreement with simulations. In fact, comparing the last two figures in the lower part of Fig. 3, we obtain a velocity of 2.1 cells per step, four times the value obtained for the axial gradient. This velocity enhancement is attributable to the fact that the spiral tip, while it is driven out of the medium in a screw-like fashion, encounters more often a driving light gradient when this gradient is radial than when the gradient points solely in one spatial direction.

The results presented here are at least qualitatively related to wave dynamics in heart muscle, as excitable media share some common fundamental properties (*1*, *3*). Measurements in vivo (*2*) and in isolated heart muscle (*4*) indicate that spiral formation is the cause of arrhythmic diseases. Moreover, simulations of heart muscle with partial differential equations (*17*) have shown that a gradient of refractoriness causes spiral drift. It has been suggested (*18*) that the traditional treatment, which consists of depolarizing shocks in the kilovolt range, may be replaced by implantable defibrillators operating at much lower potentials. In addition, the ability to control spiral drift in excitable media may find application in parallel processing with photochemical computational devices (*9*–*11*, *19*).

REFERENCES AND NOTES

1. A. V. Holden, M. Markus, H. G. Othmer, Eds., *Nonlinear Wave Processes in Excitable Media* (Plenum, New York, 1990); H. L. Swinney and V. I. Krinsky, Eds., *Waves and Patterns in Chemical and Biological Media* [*Physica D* 49 (nos. 1 and 2) (1991)].
2. K. I. Allessie, F. I. M. Bonke, F. J. G. Schopman, *Circ. Res.* **33**, 54 (1973); *ibid.* **39**, 168 (1976); *ibid.* **41**, 9 (1977).
3. J. Jalife, Ed., *Mathematical Approaches to Cardiac Arrhythmias* [*Ann. N.Y. Acad. Sci.* **561** (1990)].
4. J. M. Davidenko, P. Kent, J. Jalife, *Physica D* **49**, 182 (1991); J. M. Davidenko, A. M. Pertsov, R. Salomonsz, W. Baxter, J. Jalife, *Nature* **355**, 349 (1992).
5. G. Gerisch, *Naturwissenschaften* **58**, 430 (1971); P. Foerster, S. C. Müller, B. Hess, *Development* **109**, 11 (1990).
6. A. Gorelova and J. Bures, *J. Neurobiol.* **14**, 353 (1983).
7. R. J. Field and M. Burger, Eds., *Oscillations and Traveling Waves in Chemical Systems* (Wiley, New York, 1985).
8. S. C. Muller, Th. Plesser, B. Hess, *Science* **230**, 661 (1985); P. Foerster, S. C. Müller, B. Hess, *ibid.* **241**, 685 (1988).
9. L. Kuhnert, *Nature* **319**, 393 (1986).
10. ———, K. I. Agladze, V. I. Krinsky, *ibid.* **337**, 244 (1989).
11. Ch. Zülicke, W. Ebeling, L. Schimansky-Geier, *BioSystems* **22**, 261 (1989).
12. K. I. Agladze, V. A. Davydov, A. S. Mikhailov, *JETP Lett.* **45**, 768 (1988).
13. P. K. Brazhnik *et al.*, *Izv. Vyssh. Uchebn. Zaved. Radiofiz.* **31**, 574 (1988).
14. M. Markus and B. Hess, *Nature* **347**, 56 (1990).
15. B. F. Madore and W. L. Freedman, *Science* **222**, 615 (1983); A. T. Winfree, E. M. Winfree, H. Seifert, *Physica D* **17**, 109 (1985).
16. M. Gerhardt and H. Schuster, *Physica D* **36**, 209 (1989); ———, J. J. Tyson, *Science* **247**, 1563 (1990).
17. A. V. Panfilov and B. N. Vasiev, *Chaos, Solitons, Fractals* **1**, 119 (1991).
18. A. T. Winfree, *Ann. N.Y. Acad. Sci.* **561**, 190 (1990).
19. H. Haken, *J. Chem. Phys.* **84**, 1289 (1988); *Z. Phys.* **470**, 121 (1988); W. Ebeling, *J. Stat. Phys.* **45**, 891 (1986).
20. This work is part of Study Project PS* 0303 of the Commission of the European Communities (Brussels). We thank W.-D. Sponheimer and H. Schepers for computational assistance and J. Ungvarai for help in carrying out the experiments.

15 January 1992; accepted 7 May 1992

Kinetics of the OH Reaction with Methyl Chloroform and Its Atmospheric Implications

Ranajit K. Talukdar, Abdelwahid Mellouki,* Anne-Marie Schmoltner,
Thomas Watson, Stephen Montzka, A. R. Ravishankara†

The rate coefficients for the reaction of hydroxyl (OH) radicals with methyl chloroform (CH_3CCl_3) were measured between 243 and 379 kelvin with the pulsed photolysis–laser-induced fluorescence method. The measured rate coefficients at 298 and 277 kelvin were ~20 and ~15%, respectively, lower than earlier values. These results will increase the tropospheric OH concentrations derived from the CH_3CCl_3 budget analysis by ~15%. The predicted atmospheric lifetimes of species whose main loss process is the reaction with OH in the troposphere will be lowered by 15% with consequent changes in their budgets, global warming potentials, and ozone depletion potentials.

Methyl chloroform (CH_3CCl_3) is exclusively man-made. Its rate of release into the atmosphere can be accurately estimated from industry production figures (*1*), and its atmospheric loss is due primarily to reaction with OH radicals. [Recently, oceanic consumption has been identified as an additional small loss process accounting for about 7% of the total CH_3CCl_3 removal (*2*).] Therefore, measurements of atmospheric CH_3CCl_3 concentrations have been used to deduce globally averaged tropospheric OH concentrations (3), which in turn are used to calculate atmospheric lifetimes of species such as methane (CH_4) and haloethanes, which are used as chlorofluorocarbon (CFC) substitutes. The OH concentrations calculated from the CH_3CCl_3 budget analysis critically depend on the rate coefficient, k_1, for the reaction

$$OH + CH_3CCl_3 \rightarrow H_2O + CH_2CCl_3 \quad (1)$$

The generally accepted value of k_1 (*4*, *5*) is based on the results of Kurylo *et al.* (*6*) and Jeong and Kaufman (*7*), which are in good agreement with each other between 278 and 363 K. Investigations carried out earlier than these two studies reported significantly

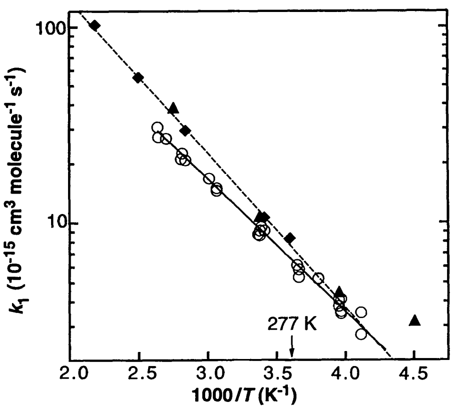

Fig. 1. Plot of ln k_1 versus $1/T$ measured in this study (open circles), by Kurylo *et al.* (*6*) (triangles), and by Jeong and Kaufman (*7*) (diamonds). The solid line is a fit of our data to an Arrhenius expression. The dashed line represents the recommendations of the National Aeronautics and Space Administration (*4*) and the International Union of Pure and Applied Chemistry (*5*) that are currently used in atmospheric calculations.

higher values, which were erroneous for reasons discussed by Kurylo *et al.* and Jeong and Kaufman.

The direct determinations of k_1, that is, without reference to another rate coefficient, have been carried out using the flow tube or pulsed photolysis method. Because in these methods the loss of OH reactant is measured in an excess of CH_3CCl_3, there are two potential sources of error. First, stabilizers and contaminants in the CH_3CCl_3 sample can also react with the OH radicals. Stabilizers, such as 1,4-dioxane, are added to CH_3CCl_3 samples to prevent its decomposition and they react rapidly with OH. The common contaminant CH_2CCl_2 is a by-product of CH_3CCl_3 production and is also produced by its decomposition; hence, it is usually present in CH_3CCl_3 samples. The rate coefficient for the reaction of OH with CH_2CCl_2 is $>10^4$ times k_1. Second, significant concentrations of free radicals may be produced by the reaction of CH_3CCl_3 with OH. These free radicals can enhance the observed OH removal rates; if so, the measured rate coefficients will be higher than the true values (*8*). In the pulsed photolysis experiments, there may be an additional complication due to the photolysis of CH_3CCl_3 and the reactions of photolytic products with OH.

We measured k_1 using the pulsed photolysis–laser-induced fluorescence method, taking great care to identify and minimize the problems mentioned above. The apparatus and experimental procedures are described elsewhere (*9*). We used various OH sources (*10, 11*): (i) 355-nm laser photolysis of HONO, (ii) 248-nm laser photolysis of H_2O_2 and HNO_3, and (iii) broad-band (Xe flash lamp, wavelengths >165 nm) photolysis of HNO_3 and H_2O. CH_3CCl_3 does not absorb at 355 nm. Its absorption cross section at 248 nm is ~2×10^{-22} cm^2. Therefore, CH_3CCl_3 photolysis was not a problem in these studies. The third source was used to investigate if substantial differences would be observed when CH_3CCl_3 was also photolyzed.

We monitored the relative OH concentrations, by using pulsed laser-induced fluorescence, as a function of time between the photolysis and probe laser pulses. The concentration of CH_3CCl_3 was typically $>10^5$ times that of OH. The concentration of CH_3CCl_3 flowing through the reactor was measured by absorption at 214 nm (Zn lamp) in cells located ahead of and behind the reactor. Thus, the required CH_3CCl_3 concentration was directly measured. Any significant loss (>2%) of CH_3CCl_3 to the walls or to heterogeneous decomposition would have been detected. It is important to know this concentration because the uncertainty in k_1 is directly proportional to the uncertainty in the CH_3CCl_3 concentration. We measured the absorption cross section of CH_3CCl_3 at 214 nm, which is needed to determine its concentration, to be $(1.33 \pm 0.05) \times 10^{-19}$ cm^2. The uncertainty represents a combination of random and systematic errors at the 95% confidence level. The major systematic errors in this measurement are in the pressure measurements, the adsorption of CH_3CCl_3 on the absorption cell windows, and the presence of absorbing impurities. We measured the cross section using two absorption cells (100 and 25 cm long); the cell was either filled with CH_3CCl_3 or CH_3CCl_3 flowed through the cell at known pressures. In all cases, the Beer-Lambert law was strictly

Table 1. Summary of experimental conditions and the measured values of k_1 as a function of temperature. Quoted error bars are 2σ and do not include estimated systematic errors. Cell pressure, 25 to 75 torr; flow velocity through the interaction zone, 4 to 10 cm s^{-1}.

Temperature (K)	OH source	$[OH]_0$ (10^{10} cm^{-3})	$[CH_3CCl_3]$ range (10^{15} cm^{-3})	$[CH_2{=}CCl_2]$ (ppmv)	k_1 (corrected) (10^{-14} cm^3 molecule^{-1} s^{-1})
233	HONO	36	24–101	8	0.304 ± 0.019
233	H_2O_2	8	25–83	12	0.267 ± 0.018
243	HONO	38	17–100	31	0.270 ± 0.019
243	H_2O_2	6	23–90	7	0.349 ± 0.016
252	HONO	34	17–119	42	0.355 ± 0.026
252	HONO	19	11–98	31	0.346 ± 0.030
252	H_2O_2	11	15–107	12	0.410 ± 0.013
253	HONO	12–29	30–110	2	0.405 ± 0.017
253	H_2O_2	4	22–104	33	0.377 ± 0.018
263	HONO	44	23–122	8	0.522 ± 0.030
263	H_2O_2	5	14–93	19	0.520 ± 0.022
273	HONO	16	11–126	12	0.579 ± 0.022
273	HONO	23	14–114	42	0.530 ± 0.026
274	H_2O_2	7	14–85	30	0.609 ± 0.030
293	H_2O	10	8–101	15	0.898 ± 0.064
295	H_2O_2	7	14–80	20	0.899 ± 0.100
296	H_2O_2	4	16–92	40	0.910 ± 0.030
296	HONO	27	11–123	12	0.859 ± 0.027
297	HONO	23	13–94	20	0.851 ± 0.023
326	HONO	16	10–80	2	1.49 ± 0.05
326	H_2O	10	10–85	9	1.44 ± 0.10
332	H_2O_2	7	12–78	20	1.65 ± 0.05
352	HONO	23	9–83	2	2.07 ± 0.06
355	H_2O	10	9–77	5	2.24 ± 0.11
356	HONO	31	10–97	20	2.08 ± 0.08
370	HNO_3	20	5–59	6	2.67 ± 0.05
378	HONO	29	9–70	2	2.71 ± 0.05
379	H_2O	10	6–71	20	3.05 ± 0.11

R. K. Talukdar, A. Mellouki, A.-M. Schmoltner, T. Watson, National Oceanic and Atmospheric Administration, Environmental Laboratories, Aeronomy Laboratory, Boulder, CO 80303 and Cooperative Institute for Research in Environmental Sciences, University of Colorado, Boulder, CO 80309.

S. Montzka, Climate and Diagnostic Laboratory, National Oceanic and Atmospheric Administration, Boulder, CO 80303

A. R. Ravishankara, National Oceanic and Atmospheric Administration, Environmental Laboratories, Aeronomy Laboratory, Boulder, CO 80303 and Cooperative Institute for Research in Environmental Sciences and Department of Chemistry and Biochemistry, University of Colorado, Boulder, CO 80309.

*Present address: Laboratoire de Combustion et Systémes Réactifs/Centre National de la Recherche Scientifique, 45071 Orleans Cedex 02, France.

†To whom correspondence should be addressed at NOAA/ERL, R/E/AL2, 325 Broadway, Boulder, CO 80303.

Table 2. Comparison of results from recent investigations of k_1 and currently recommended values. All errors are those quoted by the authors.

$k_{1(298\text{ K})}$ (10^{-14} cm^3 s^{-1})	A (10^{-12} cm^3 s^{-1})	($E/R \pm \Delta E/R$) (K)	T range (K)	Technique*	Reference
1.16 ± 0.10†	5.41 ± 1.84	1831 ± 95	278–457	DF-RF	(*7*)
1.12 ± 0.21†	5.40 ± 1.8	1810 ± 100	222–363	FP-RF	(*6*)
1.30 ± 0.30	5.4 ± 3.0	1803 ± 450	359–402	PR-UVKS	(*16*)
1.09 ± 0.35			298	Relative rate‡	(*16*)
1.2	5.0	1800 ± 200	250–460	Rec.	(*4*)
1.2	5.1	1800 ± 200	250–460	Rec.	(*5*)
0.95 ± 0.08	1.75 ± 0.34	1550 ± 60	233–379	PP-LIF	This work

*DF-RF, discharge flow–resonance fluorescence; FP-RF, flash photolysis–resonance fluorescence; PR-UVKS: pulsed radiolysis–ultraviolet kinetic spectroscopy; PP-LIF, pulsed photolysis–laser-induced fluorescence; Rec., recommended. †These are scaled to 298 K using E/R = 1550 K. ‡Measured relative to the reaction of OH with CH_3Cl assuming a rate coefficient for that reaction of 1.36 × 10^{-14} cm^3 molecule^{-1} s^{-1}.

obeyed, and the results agreed to within 0.5%. The capacitance manometer used for pressure measurements is accurate to better than 1%. The levels of impurities in our samples were in the parts per million by volume (ppmv) range. Therefore, we conservatively estimate the uncertainty in the cross sections as ~3.5%. Our value is close to that reported earlier (*12*) [(1.23 ± 0.02) × 10^{-19} cm^2]. We used the measured value to calculate the CH_3CCl_3 concentrations.

Nonstabilized CH_3CCl_3 obtained from Dow Chemicals was purified by passing He through it until >70% of the sample was removed. The main impurities in our sample, CH_2Cl_2, $CHCl_2CH_3$, and $CHClCCl_2$, were identified and quantified by gas chromatography (with flame ionization or mass spectrometric detection). The levels of CH_2Cl_2, the major impurity, varied between 2 and 42 ppmv in different samples and also with time in the same sample. For measurements below 298 K (where the interference from CH_2Cl_2 is more pronounced), we frequently checked for the levels of CH_2Cl_2. The rate coefficient for the OH + CH_2Cl_2 reaction [(2.36 ± 0.16) × 10^{-12} exp[(450 ± 20)/T] cm^3 s^{-1}] was measured recently in this laboratory (*13*) under the pressure and gas composition conditions used here and was used to correct the measured values of k_1. The corrections varied with the sample purity, increased with decreasing temperature (T), and were negligible above 298 K. Typically, the corrections were a few percent. In one case the correction was as high as 17%. The levels of $CHCl_2CH_3$ and $CHClCCl_2$ were always less than 10 ppmv and, on the basis of the rate coefficient for their reactions with OH (*14*), they contributed negligibly to the measured k_1.

The values of k_1 measured between 233 and 379 K (Table 1 and Fig. 1) were independent of total pressure (25 to 75 torr), flow rate (4 to 10 cm s^{-1}), photolysis laser fluence (5 to 20 mJ cm^{-2} at 248 nm and 15 to 40 mJ cm^{-2} at 355 nm), and the OH sources. The data between 243 and 379 K are well represented by the expression: (1.75 ± 0.34) × 10^{-12} exp[−(1550 ± 60)/T] cm^3 s^{-1}. (The quoted uncertainties are at the 95% confidence level for each of the parameters and do not include estimated systematic errors.) The above Arrhenius parameters are not significantly different from those obtained by an analysis of our data between 298 and 379 K and thus confirm the negligible contributions of the impurity reactions to the measured value of k_1. (Data obtained at 233 K were not included in this analysis because of the wider spread in the measured values and the larger difficulties associated with their measurements.) The parameters and uncertainties needed to calculate values of k_1 for atmospheric modeling are more appropriately presented (*4*, *5*) as: k_1(298 K) = 9.5 × 10^{-15} cm^3 s^{-1}; A = 1.75 × 10^{-12} cm^3 s^{-1}; E/R = 1550 K (where A is the Arrhenius A-factor, E is the activation energy, and R is the gas constant). The uncertainty, at the 95% confidence level, for the 298 K value is a factor f(298) = 1.08. At other temperatures the uncertainty factor $f(T)$ for k_1 calculated from the above Arrhenius parameters is given by

$$f(T) = f(298\text{ K}) \exp\left[(\Delta E/R)\left(\frac{1}{T} - \frac{1}{298}\right)\right] \qquad (2)$$

where $\Delta E/R$ = 100 K. The above error bounds account for the uncertainties in the ultraviolet (UV) absorption cross section at 214 nm, the difference between the value of k_1 calculated from the Arrhenius parameters and the value measured near 298 K (after correction for small differences in temperature), and the uncertainty in the temperature dependence of k_1. The k_1(298 K) quoted above is the average of the value measured near 298 K and that calculated from the Arrhenius expression (which agree to within 4%).

Our values at 298 K (Table 2 and Fig. 1) and 277 K (Fig. 1) are 22 and 16%, respectively, lower than the recommendations (*4*, *5*) that are based on results of Kurylo *et al.* (*6*) and Jeong and Kaufman (*7*). However, they do overlap with the recommended values within their quoted uncertainties. Our results are based on analyzed samples, are corrected for impurity contribution, and are based on directly measured CH_3CCl_3 concentrations. In addition, we kept the concentrations of OH and the CH_3CCl_3 photolysis products low enough to make secondary reactions negligible. We also avoided purification that involved heating CH_3CCl_3. We have observed the decomposition of CH_3CCl_3 to form CH_2CCl_2 at about 400 K in metal tubes.

Attempts were made to understand the reasons for the discrepancies between our results and those of Kurylo *et al.* (*6*), who used a technique similar to ours. We photolyzed HNO_3 using a Xe flash lamp to produce OH, the same method as that used by Kurylo *et al.*; the OH concentration rose and then fell as a function of reaction time when CH_3CCl_3 was present. The values of k_1 obtained from the decay parts of the temporal profiles were considerably lower than those in the laser photolysis experiments. Secondary generation of OH interfered with measuring k_1, and we were unable to reproduce the results of Kurylo *et al.* Recent experiments (*15*) have shown that HNO_3 photolysis at 193 nm produces very little OH but large amounts of O atoms. Therefore, vacuum UV photolysis of HNO_3 is not a good source of OH for kinetic measurements. It is not clear if production of O atoms could have caused systematic errors in the study of Kurylo *et al.*

The measurements by Nelson *et al.* (*16*) cover only a small temperature range (359 to 402 K), and k_1 was not directly measured at or below room temperature. Their relative measurement at 298 K yields a lower value of k_1 than that calculated from their direct measurements.

The increasing discrepancy between our results and those of Kurylo *et al.*, Jeong and Kaufman, and Nelson *et al.* with increasing temperature is opposite to what is expected if reactive impurities were present in CH_3CCl_3 samples used by these investigators. One possible cause for the disparity is the decomposition of CH_3CCl_3 at higher temperatures to produce the reactive CH_2CCl_2 in earlier studies. The decomposition of CH_3CCl_3 is quite rapid over Al surfaces and is the main reason for adding inhibitors to the commercial samples of CH_3CCl_3. Also, we observed decomposition of CH_3CCl_3 when it was heated in stainless steel tubes up to 400 K for a few minutes. (We found that CH_3CCl_3 samples stored in glass containers at 273 K were stable for at least 8 months as shown by the invariance of k_1 measured using the same sample but 8 months apart.) In some of the earlier studies, CH_3CCl_3 may have decomposed upon heating or on metal cell walls. We also have observed that the formation of CH_2CCl_2 is enhanced in the presence of water adsorbed on surfaces. Nelson *et al.* (*16*) used approximately 12 torr of H_2O to produce OH, and they could have inadvertently generated CH_2CCl_2.

Our results indicate that the previously accepted values of k_1 are too high above 240 K. The lower values of k_1 at tropospheric temperatures increase the OH concentrations estimated from the CH_3CCl_3 budget analysis. This increase, in turn, decreases the calculated tropospheric lifetimes of molecules whose primary loss is via reaction with OH. The magnitude of the change can be roughly gauged from the values of k_1 at 277 K, which is an approximate average of the temperature at which the OH-initiated degradation of a well-mixed tropospheric gas takes place. Our value of k_1 at 277 K is ~15% lower than the earlier recommendations. Examples of the implications of the new value of k_1 include (i) a decrease in the calculated atmospheric lifetime of CH_4 by 15% and a 15% increase in its flux to balance the larger atmospheric loss rate, and (ii) decreases in the calculated lifetimes of hydrofluorocarbons and hydrofluorochlorocarbons (HCFCs) and ozone depletion potentials of HCFCs, the proposed CFC substitutes, by 15%. In the case of CH_4, the new value of k_1 will partially offset the balance in its budget that was calculated after our report on the OH + CH_4 reaction (*8*).

Note added in proof: DeMore (*17*) and Finlayson-Pitts *et al.* (*18*) have also recently measured k_1 to be substantially the same as that reported here

REFERENCES AND NOTES

1. P. Midgley, *Atmos. Environ.* **23**, 2663 (1989).
2. J. H. Butler *et al.*, *J. Geophys. Res.* **96**, 22347 (1991).
3. R. Prinn *et al.*, *ibid.* **97**, 2445 (1992).
4. W. B. DeMore *et al.*, *Chemical Kinetics and Photochemical Data for Use in Stratospheric Modeling* (Evaluation No. 9, JPL Publ. 90-1, Jet Propulsion Laboratory, Pasadena, CA, 1 January 1990).
5. R. Atkinson *et al.*, *J. Chem. Phys. Ref. Data* **18**, 881 (1989).
6. M. J. Kurylo, P. C. Anderson, O. Klais, *Geophys. Res. Lett.* **6**, 760 (1979).
7. K.-M. Jeong and F. Kaufman, *ibid.*, p. 757.
8. G. L. Vaghjiani and A. R. Ravishankara, *Nature* **350**, 1 (1991).
9. ______, *J. Phys. Chem.* **93**, 1948 (1989).
10. T. Gierczak, R. Talukdar, G. L. Vaghjiani, E. R. Lovejoy, A. R. Ravishankara, *J. Geophys. Res.* **96**, 5001 (1991).
11. A. Wahner and A. R. Ravishankara, *ibid.* **92**, 2189 (1987).
12. N. Vanlaethem-Meurée, J. Wisemberg, P. C. Simon, *Geophys. Res. Lett.* **6**, 451 (1979).
13. R. K. Talukdar, A. Mellouki, A. R. Ravishankara, in preparation.
14. The rate coefficient for the reaction of OH with 1,1-dichloroethane cannot be larger than that for the reaction of OH with C_2H_6. We have used the rate coefficient for the OH + C_2H_6 reaction (*4*) in placing the limit for the contribution of the OH + 1,1-dichloroethane reaction to the measured value of k_1. The rate coefficient for the reaction of OH with $CHClCCl_2$ is from (*4*).
15. A. A. Turnipseed, G. L. Vaghjiani, J. E. Thompson, A. R. Ravishankara, *J. Chem. Phys.* **96**, 5887 (1992).
16. L. Nelson, I. Shanahan, H. W. Sidebottom, J. Treacy, O. J. Nielsen, *Int. J. Chem. Kinet.* **22**, 577 (1990).
17. W. DeMore *Geophys. Res. Lett.*, in press.

18 B. J. Finlayson-Pitts *et al.*, *ibid.*, in press.

19. This research was funded in part by the National Oceanic and Atmospheric Administration's climate and global change program. We are grateful to Dow Chemicals and C. Nieme for the analyzed samples of CH_3CCl_3.

30 March 1992; accepted 18 May 1992

Microaggregations of Oceanic Plankton Observed by Towed Video Microscopy

Cabell S. Davis, Scott M. Gallager, Andrew R. Solow

Oceanic plankton have been hypothesized to occur in micropatches (<10 meters) that can have a large impact on marine ecosystem dynamics. Towed video microscopy was used to unobtrusively determine distributions of oceanic plankton over a continuum of scales from microns to hundreds of meters. Distinct, taxa-specific aggregations measuring less than 20 centimeters were found for copepods but not for nonmotile (cyanobacterial colonies) or asexual (doliolid phorozooids) forms, which suggests that these small patches are related to mating. Significant patchiness was also found on larger scales and was correlated among taxa, indicating physical control. These video observations provide new insights into basic plankton ecology by allowing quantitative assessment of individual plankton in their natural, undisturbed state.

The microscale (<10 m) environment of oceanic plankton is thought to be important in determining population and ecosystem dynamics (*1, 2*). Foraging models have shown that microscale patchiness in prey density can greatly enhance predator population growth (*3, 4*). In laboratory experiments, the abundance of prey required for maximal growth of predators is often well above that found in the field; the body size and the growth rate of field predators, however, are similar to those of laboratory animals grown in saturating food (*1, 5*). This discrepancy is hypothesized to be a result of field predators feeding in micropatches of prey that are too small to resolve with existing instrumentation (*1, 4–6*).

Spatial distributions in oceanic plankton on scales from microns to hundreds of meters were determined with the use of the newly developed video plankton recorder (VPR) (*7*). The VPR was equipped with conductivity, temperature, pressure, and flow sensors and was towed at 0.75 to 2.25 m/s near the surface (1 to 8 m) and outboard (7 m) of the side of the ship. Video recordings were scanned visually at 5 to 30 fields per second to detect the presence of organisms, and when they were found, taxa and time code were noted. Tow speed data from the flow sensor were used to convert the time code to distance along the tow path.

Tows were made from the R.V. *Oceanus* on 29 and 30 August 1991 in continental shelf (70 m bottom depth; 40°41′N, 70°33′W) and slope (39°32′N, 70°00′W) waters south of Woods Hole, Massachusetts. A tow from each area was analyzed for the presence of micropatchiness. Satellite infrared imagery together with VPR data on sea surface temperature and salinity indicated the slope station was positioned in the western edge of a warm-core Gulf Stream ring. Seas were calm, with the result that the wind-induced turbulent mixing rate was minimal, favoring micropatch formation (*4*).

The unobtrusive nature of the VPR (*8*) enabled observation and quantification of delicate forms that have typically been difficult or impossible to sample with traditional gear such as nets, pumps, and Niskin bottles. These forms included cyanobacterial colonies (Fig. 1A), marine snow, copepods carrying egg clutches, doliolids with buds (Fig. 1B), medusae, ctenophores, larvaceans (Fig. 1F), sarcodines, salp chains, and large, chain-forming diatoms. Such forms can have a large impact on marine ecosystem dynamics, but little is known of their abundance and distribution. Large amounts of nitrogen-fixing cyanobacterial colonies, *Trichodesmium* sp. (Fig. 1A), were found along the transect in the warm-core ring (Fig. 2), which supports the view that they are potentially a major source of new nitrogen and organic carbon in open ocean areas (*9*). Likewise, gelatinous forms such as the tunicate *Doliolum nationalis* (Fig. 1B) were found in dense patches along the

---

C. S. Davis and S. M. Gallager, Department of Biology, Woods Hole Oceanographic Institution, Woods Hole, MA 02543.
A. R. Solow, Department of Marine Policy, Woods Hole Oceanographic Institution, Woods Hole, MA 02543.